Remote Sensing of Ocean Waves and Currents Using AIRSAR Along-Track Interferometry (ATI)

Duk-jin Kim[1], **and Wooil M. Moon**[1,2]
1. ESI[3] Laboratory, School of Earth & Environmental Science
Seoul National University, Seoul 151-742, Korea
2. Geophysics, University of Manitoba, Winnipeg, MB R3T 2N2, Canada
(djkim@eos1.snu.ac.kr, wmoon@cc.umanitoba.ca)

David A. Imel, and Delwyn Moller
Radar Science and Engineering Section, Jet Propulsion Laboratory
4800 Oak Grove Drive Pasadena, CA 91109
(imel@jpl.nasa.gov, Delwyn.Moller@jpl.nasa.gov)

Abstract

The phase information in along-track interferometry (ATI) SAR images is a measure of the Doppler shift of the backscattered signal and thus of the line-of-sight velocity of the scatterers. This interferometric velocity is the sum of the orbital motion of water particles from the swell, phase velocities of the Bragg waves, and ocean surface currents. While the advent of ATI SAR provided us with a potentially powerful technique for ocean current mapping, the surface currents cannot yet measured exactly from interferometric velocity measurements. In this paper, we will apply a new method of extracting the surface current velocity from multiple-frequency (L- & C-band) ATI SAR data.

We have tested ATI SAR data that were collected during the PACRIM-II AIRSAR experiment over the Ulsan coast on the southeastern part of the Korean peninsula. Two lines of ATI data were collected at right angle on September 30th, 2000. We have investigated the ocean waves and current features and have retrieved dominant ocean wave spectrum. The dominant wavelength of swell stays constant over most parts of the study area, but the variation of bottom topography refracts the propagation direction of ocean waves. Furthermore, we could differentiate the ocean current and the Bragg wave phase velocities using multiple-frequency (C & L-band) ATI data.

I. INTRODUCTION

The conventional SAR intensity image over ocean surfaces has some limitations in obtaining quantitative information such as current velocity and wave height, because the radar modulation transfer function (MTF) over ocean waves is not understood. Recently, airborne Along-Track Interferometric (ATI) SAR has been actively investigated, which has the potential of measuring ocean surface currents and waves [1], [2], [3]. However, the correct surface current and Bragg wave phase velocities could not be extracted from ATI data. The ATI SAR employs two antennas that are separated physically along the platform flight path (along track) direction.

In this paper, we have tested PACRIM-II AIRSAR ATI data that were collected over the Ulsan coast, off the southeast shore of the Korean peninsula. Two lines of ATI data were collected at right angles on September 30th, 2000. We have investigated the propagation direction and velocity of dominant ocean waves considering the effect of bottom topography. This paper also describes a method briefly for extracting the ocean current and Bragg wave phase velocities using multiple-frequency (C- & L-band) ATI data.

II. ALONG TRACK INTERFEROMETRY

A. Basic principle of ATI

The geometry for the Along Track Interferometry (ATI) is schematically outlined in Fig. 1. Here, x denotes the coordinate in azimuth (along-track) direction and y denotes the coordinate in ground range (cross-track) direction. The flight direction of the platform carrying the along-track antennas is in the x direction and these two antennas are separated by a distance B

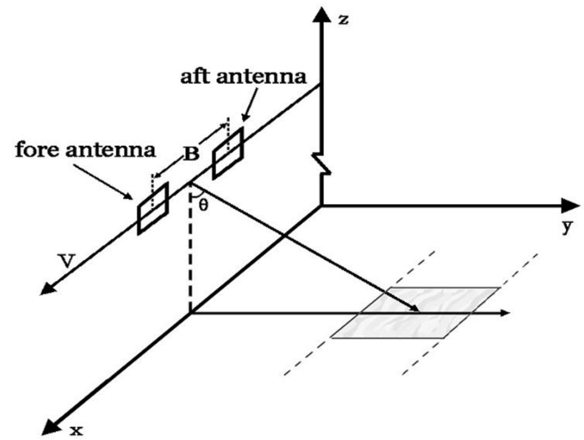

Fig. 1. Schematic geometry of the ATI (Along-Track Interferometry)

in the along-track direction. Since the platform moves with the velocity V , the image of an identical surface area is obtained by the two antennas separated by distance $\Delta x = B$ with the time interval $\Delta t = B/2V$. This depends on ATI operating modes. In this case, the aft antenna transmits radar signals and both antennas receive the backscattered signals. The phase difference Δf between the returned signals at the two antennas, which is due to the Doppler shift w_D and the time interval Δt , is related to the measured radial component of the surface velocity U_r by

$$\Delta f = w_D \Delta t = \frac{kB}{V} \cdot U_r = \frac{2pB}{l V} \cdot U_r \qquad (1)$$

where k and l are the radar wave vector and wavelength respectively. The radial component of the surface scatterers velocity (U_r) represents the vector sum of the surface current, the orbital velocity of the swell and the phase velocities of the Bragg-resonant waves [1].

B. Surface current estimation using multiple-frequency ATI SAR data

The measurement made with the ATI SAR is a measure of the surface Doppler velocity, which is a sum of the line-of-sight velocities within a given resolution cell of the radar. The ocean surface Doppler velocity measurement is composed of several contributions

$$U = v_c + v_o + v_b \qquad (2)$$

where v_c represents the surface current, v_o is the orbital velocity of the swell, and v_b is the phase velocities of Bragg-resonant waves.

To obtain the surface current from the Doppler velocity measurement, the contributions, v_o and v_b , must be extracted. Since Bragg scattering theory specifies that the radar is primarily sensitive to radially traveling waves satisfying the Bragg resonance condition for a given viewing direction, the relative spectral densities of approaching and receding waves are used to determine v_b [5]

$$\begin{aligned} v_b(q_w) &= a(q_w)c_p - [1 - a(q_w)]c_p \\ &= [2a(q_w) - 1] \cdot c_p \end{aligned} \qquad (3)$$

where a and $1-a$ represent the respective proportions of approaching and receding Bragg-resonant wave spectra density contributing to the radar echo. To use this equation, we should know the wind direction relative to radar look-direction in order to estimate Bragg-resonant phase velocity. However, simultaneous field observation of wind direction cannot always be achieved. More general solution resolving this problem was introduced by Kim et al. [3]. They assumed that the respective proportion of approaching Bragg-resonant waves (a) corresponding to two frequencies is almost equivalent. Under this assumption, they developed the following relationship. In Equation (2), the averaged velocity, $\langle U \rangle$, over large areas (v_o is removed by averaging) is the sum of Bragg wave phase velocities (v_b) and ocean surface current (v_c). The Bragg wave phase velocities depend on radar frequency, while ocean surface current velocity is steady over relatively wide area regardless of radar frequency. Therefore, we can infer that the difference between L-band and C-band averaged velocities is caused by the difference of Bragg-resonant wave phase velocities. These conditions satisfy the equation [3]

$$\begin{aligned} \langle U \rangle^L - \langle U \rangle^C &= v_b^L - v_b^C \\ &= [2a^L(q_w) - 1]c_p^L - [2a^C(q_w) - 1]c_p^C \\ &= [2a(q_w) - 1](c_p^L - c_p^C) \end{aligned} \qquad (4)$$

Equation (4) states that the a value and the wind direction information can be extracted from the difference between the multiple-frequency ATI SAR data. Furthermore, one can extract the Bragg wave phase velocities and the ocean surface current ($\langle U \rangle - v_b$) at each frequency ATI SAR data.

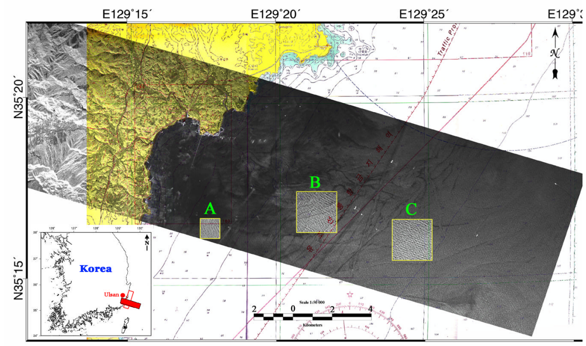

Fig. 2. Study area. The image is the magnitude image of LAA test data and topography as base map. The sub area A, B and C were selected for detail ocean wave investigation.

III. EXPERIMENTAL RESULTS

We have processed ATI data from PacRim-II mission on September 30th, 2000 over the Ulsan coast off the southeast shore of the Korean peninsula. During the PacRim-II Korea mission, two lines of ATI data were collected and the two ATI lines are approximately at right angle to each other. One flight direction was at 197°, which was approximately parallel to the coastal line, and the other flight direction was at 107°, which was perpendicular to the coastal line (Fig. 2).

Table I shows the parameters of the NASA/JPL AIRSAR during the Korean ATI experiment. The direct computation of ocean current velocities from the interferogram using Equation (1) has some problems, because the interferogram is not fully calibrated. If the scatterer elevation varies from the reference, a differential phase is introduced into the interferogram. This should have no effect on ocean scenes, but will introduce phase changes following the topography of the land in the same scene. Another significant effect on the interferogram is the flat Earth phase variation. To estimate correct current and Bragg wave phase velocity, the flat Earth phase should be removed where there is a cross-track baseline component, especially with the AIRSAR C-band ATI system. There is also unknown global phase

Table I
The NASA/JPL AIRSAR parameters during the Korean ATI data acquisition

	L-band	C-band
ATI Mode	Common-Transmitter mode (ATI2)	
Wavelength	0.242257m	0.056698m
Polarization	VV	
Pulse Bandwidth	40MHz	
Pulse duration	10μs	
Sampling Frequency	90MHz (2×complex sampling frequency)	
PRF	1108Hz	
Aircraft Speed	216m/s (197-1), 219m/s (107-1)	
Altitude	8007m (197-1), 8005m (107-1)	
Physical Baseline	19.8m	1.93m

offset, in each interferogram. This propagates into the velocity maps as an unknown velocity offset. These phase biases can be removed by subtracting the non-zero phase difference over the land near the elevation reference points in the scene.

The resulting calibrated interferometry velocities (Fig. 4) can be validated by comparing them with the velocities of moving ships that cause along-track offset from their wakes. The conventional approach of estimating moving ships' velocities, which are independent of ATI technique, was estimated from the distance between the ships and their wakes (d_x) given by [6]

$$U_r = \frac{V}{R} \cdot d_x \tag{5}$$

where U_r is the radial velocity of the moving ship, R is the ship slant range, and V is the platform velocity. Another independent estimation of the velocities of the moving ships can be obtained from the unwrapped phase of ATI SAR data using Equation (1). The unwrapped ATI phase of moving ships can easily be determined by the along-track offset. Fig. 3 is an example of the moving ships with phase differences and along-track offsets. The resulting velocities obtained from ATI phase differences and along-track offsets are summarized in Table II. To extract velocities of the moving ships, we processed the ATI SAR data with 1×6 looks (range×azimuth) which is corresponding to 3.3m in range and 3.4m in azimuth direction. This range of data resolution has ±3cm/s velocity ambiguity within a pixel dimension. From these results, one could validate that the velocities extracted from ATI SAR data

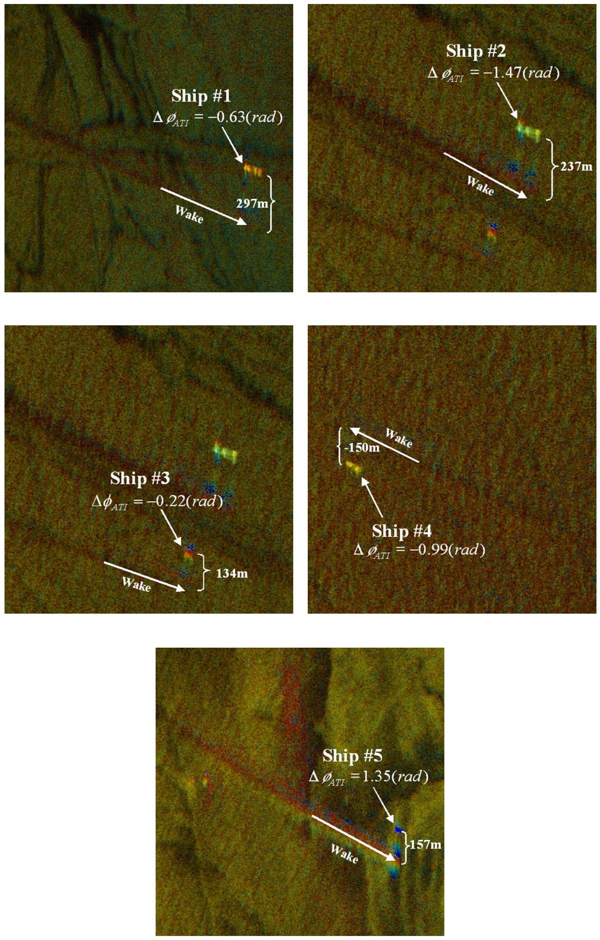

Fig. 3. These are examples of the moving ships with phase difference and along-track offset. To extract velocity of the moving ship, we have processed the ATI SAR data with 1×6 looks (range×azimuth) which is corresponding to 3.3m in range and 3.4m in azimuth direction.

Table II
This table summarizes the resulting moving ship velocities obtained from ATI phase difference and along-track offset.

	Radial Velocity of Ship: Azimuth Off-set	Radial Velocity of Ship: ATI	Difference
Ship #1	5.08 m/s	5.11 m/s	-0.03 m/s
Ship #2	4.82 m/s	4.75 m/s	0.07 m/s
Ship #3	2.76 m/s	2.60 m/s	0.16 m/s
Ship #4	-2.98 m/s	-3.11 m/s	0.13 m/s
Ship #5	3.30 m/s	3.27 m/s	0.03 m/s

are reasonable ones. In Fig. 4, one can observe the zero velocity over the land and negative velocities over the ocean in the resulting interferometry velocity map. The negative velocities over the ocean correspond to the waves or currents propagating toward the aircraft (that is, downward in this figure.). The wave-like patterns that propagate obliquely with respect to the coastal line and refraction and shoaling can also be observed as it approaches the shore.

The phase velocity of Bragg waves and the ocean current velocity are usually steady over large areas, whereas the orbital velocity due to swell is composed of the higher spatial frequencies and has a zero mean value [4]. These allow us to estimate the wavelengths and wave heights of dominant ocean waves. For the periodicity of the orbital velocity of swell, one can facilitate Fourier analysis. The wave number spectra obtained using 2-D Fourier transforms of the resulting interferometry velocity map (Fig. 4) at the sub-areas A, B, and C are illustrated in Fig. 5. As shown in this figure, one can observe a similar dominant swell wavelength of about 100m in all sub areas, but the propagation direction varies at each sub-area. This type of wave refraction can be caused by water depth variation in the off-shore Ulsan area (Fig. 6). The shallower the water depth, the slower the waves, leading to refraction of waves over shallow water depth. The waves of sub-area A experience more refraction than waves of sub-area C because of the sloping beaches and the shallow sandbank (Fig. 6). The resulting swell systems of each sub-area are summarized in Table III. The angular velocity and

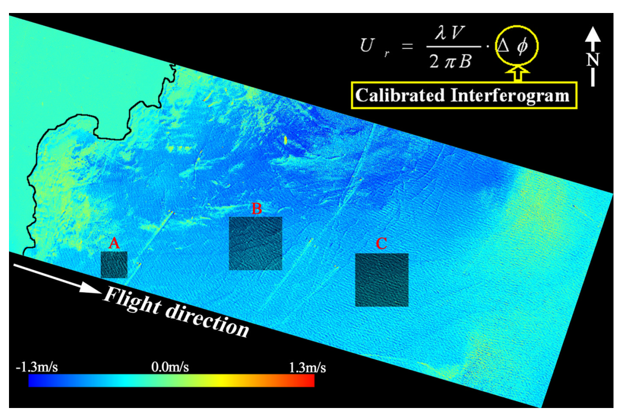

Fig. 4. Calibrated resulting interferometry velocity map calculated from ATI equation.

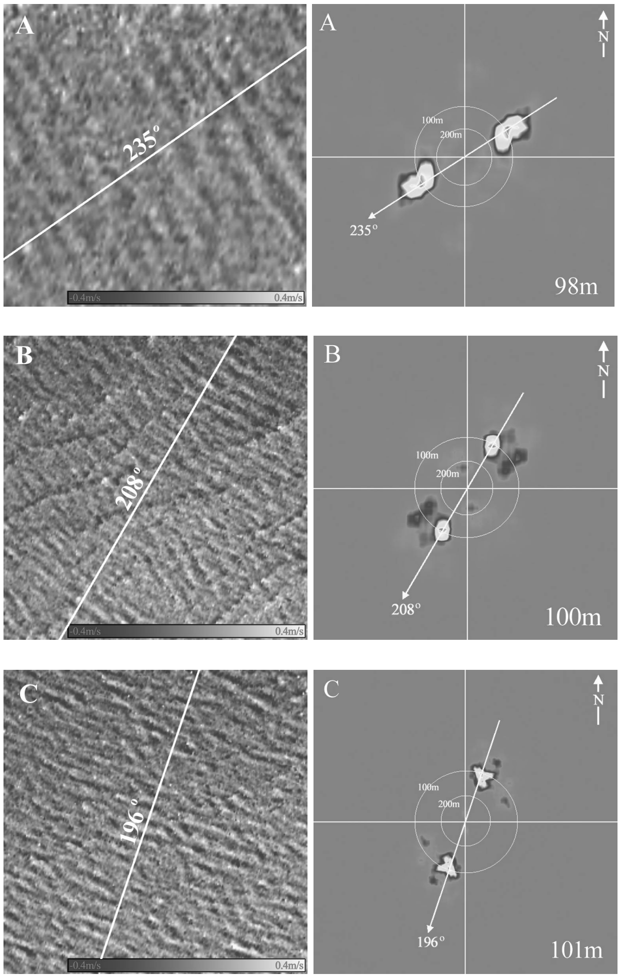

Fig. 5. Wave number spectra obtained using 2-D Fourier transform of the interferometry velocity map (Fig. 4) at the sub area A, B, and C.

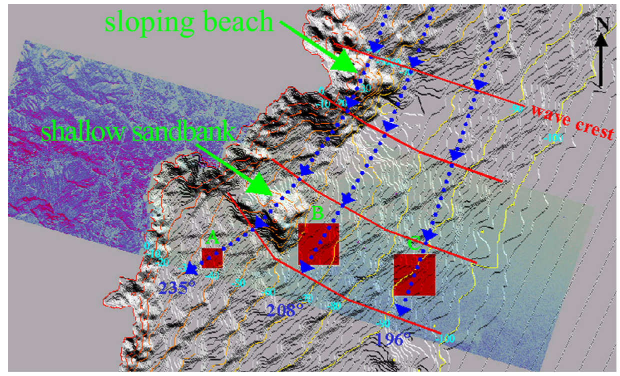

Fig. 6. This image explains the reason why the wavelength of the waves in the study area stays same whereas the propagation direction varies at each sub area. The waves of sub area A are experienced more refraction than waves of sub area C because of the sloping beaches and the shallow sandbank.

Table III
Test Results estimated from the two-dimensional wave number spectra and linear dispersion relation corresponding to sub area A, B and C.

	A	B	C
Image Size	1024m×1024m	2048m×2048m	2048m×2048m
Incidence Angle	27.0°	38.7°	38.8°
Mean Depth	-38m	-65m	-92m
Wavelength	98m	100m	101m
Wave Direction	235°	208°	196°
Wave Period	7.99s	8.01s	8.05s
Wave Velocity	12.3m/s	12.5m/s	12.5m/s

wave period are calculated using the linear dispersion relation

$$w = {}^{2p}\!/_{T} = \sqrt{kg\tanh(kh)} \qquad (6)$$

where g is the acceleration due to gravity, k is the wave number of the swell, and h is the water depth.

The radial velocity component can be appropriately transformed to real orbital velocity component of swell using the factor [7]

$$\frac{1}{G} = {}^{1}\!\Big/_{\sqrt{\sin^2 f + \cos^2 q \cos^2 f}} \qquad (7)$$

This factor is purely geometric and depends on the incidence angle (q) and the angle between the wave propagation direction and the aircraft flight direction (f).

The angular velocity of each orbiting scattering element of swell is related to the wavelength and the water depth through the linear dispersion relationship (Equation 8). Therefore, the wave height (H) can be extracted simply by dividing the twice orbital velocity with the angular velocity as follow

$$H = 2 \cdot \frac{\hat{U}_r}{G} \cdot \frac{1}{w} \qquad (8)$$

where the $\hat{U}_r$ is the amplitude of the radial velocity

The NASA/JPL AIRSAR system can acquire both the C and L-band ATI data simultaneously. So, we can differentiate the ocean current and the

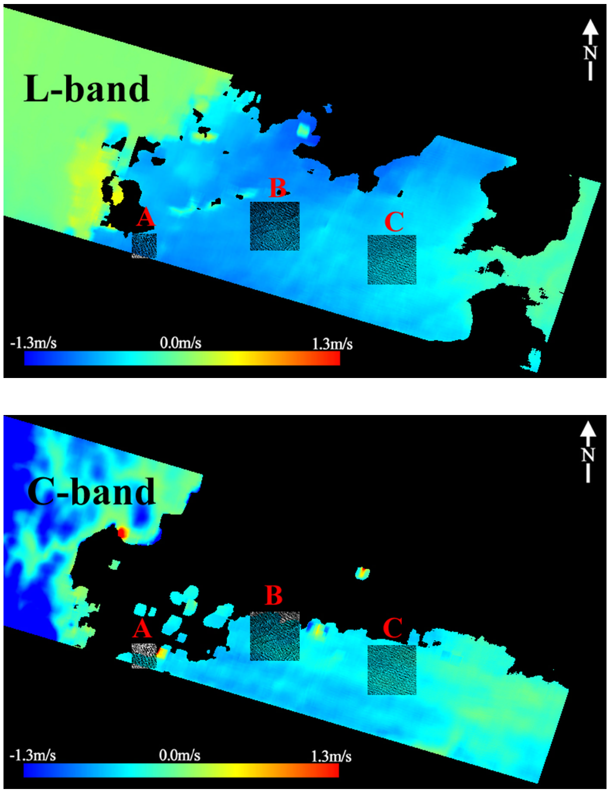

Fig. 7. Horizontal velocity map, which is sum of ocean current and Bragg wave phase velocity at each frequency data. The variation following the topography of the land in the C-band image is not arising from the motion of scatterers over the land.

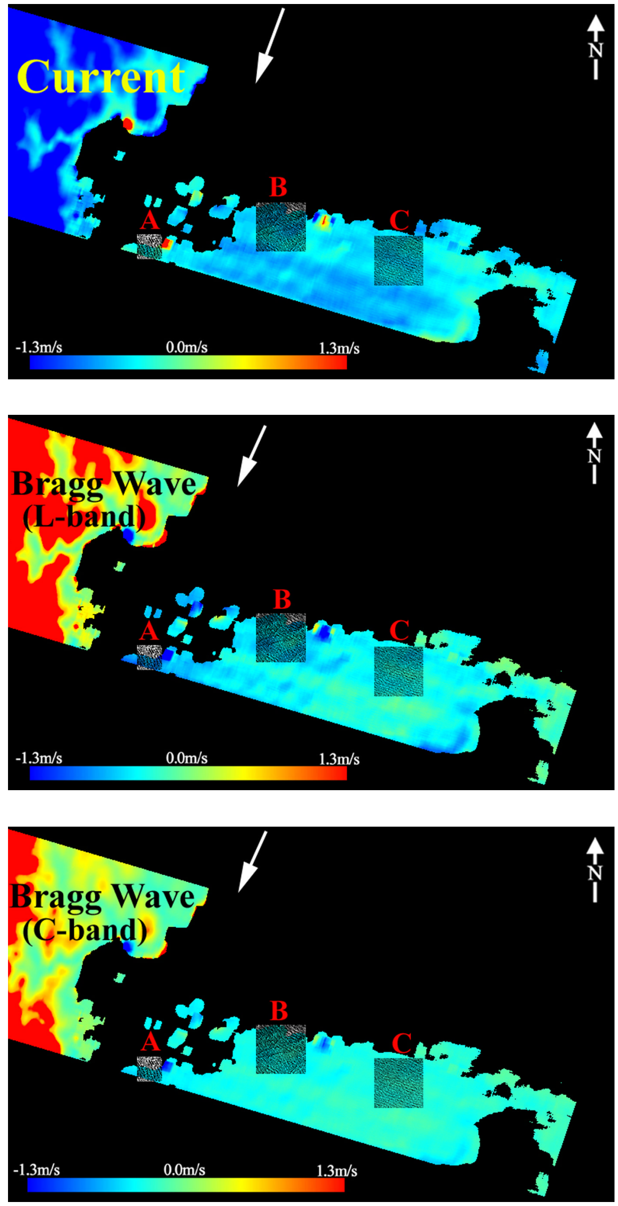

Fig. 8. These are the resulting current velocity (a) and Bragg wave phase velocities (b)(c) images extracted from multiple (L- & C-band) ATI data using Equation 6. The white arrows indicate one component direction. The results of each test sites are summarized in Table 4.

Bragg wave phase velocities from NASA/JPL ATI data using Equation (4).

Fig. 7 shows the velocities from which the periodic orbital velocity was removed at each frequency band data. These were calculated by averaging over a 400m×400m area, in which the correlation value is higher than 0.8. The rest of the areas were masked. And the radial component velocity was converted to horizontal component velocity using the equation, $\langle U_h \rangle = \langle U_r \rangle / \sin(q)$. The velocity accuracy of this ATI product is related to the signal-to-noise ratio (SNR) through the interferometric correlation

$$g_n = \frac{1}{1+SNR^{-1}} \quad \text{and} \quad g = g_n g_t \qquad (9)$$

where g_t is the temporal decorrelation of the scene, and is actually a quantity of physical interest, that is $g_t = e^{-t^2/t_c^2}$, where the t_c is the coherence time for the scattering scene. The correlation then determines the root-mean squared phase noise

$$s_f = \frac{1}{\sqrt{2N_L}} \frac{\sqrt{1-g^2}}{g} \qquad (10)$$

where N_L is the number of looks. The phase noise

Table IV
Parameters and results of test area A, B, and C for estimating the ocean current and Bragg wave phase velocity using the multi-frequency ATI data.

	A		B		C	
	L	C	L	C	L	C
Incidence Angle	27.0°		38.7°		38.8°	
$\langle U_h \rangle$	-0.68m/s	-0.51m/s	-0.65m/s	-0.49m/s	-0.53m/s	-0.42m/s
c_p	-0.65m/s	-0.31m/s	-0.55m/s	-0.27m/s	-0.55m/s	-0.27m/s
α	0.76		0.78		0.69	
Current Velocity (Range)	-0.35m/s		-0.34m/s		-0.32m/s	
Bragg Wave phase velocity	-0.33m/s	-0.16m/s	-0.31m/s	-0.15m/s	-0.21m/s	-0.10m/s

determines the minimum detectable velocity component, as well as the accuracy with which a velocity component can be measured, $\frac{lV}{2pB} \cdot s_f$. In this study area, the correlation value 0.8 can result in 4.5cm/s and 10.7cm/s of the root-mean squared velocity errors for L-band and C-band ATI data respectively.

The averaged horizontal velocity ($\langle U_h \rangle$) is the sum of Bragg wave phase velocity and ocean current. The Bragg wave phase velocity (v_b) depends on radar frequency, while ocean current velocity is steady over relatively wide area regardless of radar frequency. Therefore, one can estimate the current velocity and Bragg wave phase velocity from the difference between L-band and C-band horizontal velocities, which is caused by the Bragg wave phase velocity difference, as mentioned in section II – B, which showed that the Bragg wave phase velocities corresponding to two frequencies influence the horizontal velocity components in equal proportion. Under this assumption, we have applied the Equation (4) to the Ulsan ATI data, and obtained the surface current velocity and Bragg wave phase velocity (Fig. 8). Since only 107-1 ATI data was used in this study, we could extract only one component of the current and Bragg wave phase velocity from the ATI data. The results of each test sites are summarized in Table IV. If two orthogonal flight paths data, observing the same area, are available, it should be possible to estimate the vector of the ocean surface current and Bragg wave phase velocities.

IV. CONCLUSIONS

We used ATI SAR data that were collected during the PACRIM-II AIRSAR campaign over the Ulsan coast off the southeast shore of the Korean peninsula to investigate the ocean waves and current features.

ATI SAR employs two antennas that are separated physically along the platform flight path direction. The phase information in ATI SAR images can be transformed to interferometric velocities, which are the sums of the orbital velocity of swell, phase velocity of the Bragg wave, and ocean surface current. For the periodicity of the orbital velocity of swell, one can obtain the wavelength and the propagation direction from the 2-D Fourier transform of the resulting interferometry velocity image. Using the water depth information of the study area and the linear dispersion relationship, we were able to retrieve the period, velocity, and wave height of the swell. As for off-shore Ulsan area, excluding the immediate shoreline area, the dominant wavelength was about 100m. The wave's propagation direction was refracted towards the shoreline due to bottom topography such as sand bank or sloping beach. The dominant wave height of this area was estimated to be about 20cm.

The orbital velocity of swell can be eliminated by averaging over large areas due to its periodicity. To differentiate the phase velocity of Bragg wave and the ocean surface current from ATI SAR data, we applied a new method of using multiple-frequency (C- & L-band) ATI SAR data. The Bragg wave phase velocity depends on radar frequency used, while the ocean surface current velocity is steady over relatively wide area regardless of radar frequency. Therefore, the difference of the ATI velocity acquired by these two frequencies (L-band and C-band) over the same area is the difference of Bragg wave phase velocity resonating with each radar frequency. However, resonant-Bragg wave phase velocity measured by the radar is dictated by the ratio of the spectral densities of advancing and receding waves within the resolution cell. Because one can assume that the respective proportion of approaching (a) and receding Bragg-resonant wave spectral density contributing to the each radar frequency data are the same (Section II-B), we can calculate a value by the difference of the two frequency ATI velocity. As a result, not only that it was possible to estimate Bragg wave phase velocity, but also that it was possible to extract the surface current by subtracting the Bragg wave phase velocity from the averaged ATI velocity.

In this study, the ground truth data were limited because one of the two HF-Radar did not operate and inconsistent flight paths. Due to these circumstances, we were not able to validate the ATI data fully as we planned.

ACKNOWLEDGMENT

This research is supported by the NSERC of Canada (OG #A-7400), New Faculty Grant (SNU), and SNU Interdisciplinary Research Grant. The PACRIM-II AIRSAR Experiment was funded by SNU Interdisciplinary Grant, NSERC of Canada (Operating and Equipment Grants) and partly by Korea Research Foundation Grant (KRF-2000-015-DP0432). D. Kim was supported by the BK21 Program administered by Seoul National University. The PACRIM-II AIRSAR data processing was partly funded by Korea Aerospace Research Institute (KARI) research contract. Authors would also like to thank the PACRIM-II colleagues for the successful AIRSAR experiment.

REFERENCES

[1] R. M. Goldstein, and H. A. Zebker, "Interferometric radar measurement of ocean surface currents," Nature, Vol. 328, pp. 707-709, 1987.

[2] R. M. Goldstein, T. P. Barnett, and H. A. Zebker, "Remote Sensing of Ocean Currents," Science, Vol. 246, pp. 1282-1285, 1989.

[3] D. Kim, W. M. Moon, D. A. Imel, and D. Moller, "Investigation of Ocean Waves and Currents Using NASA (JPL) AIRSAR Along-Track Interferometry (ATI)", IEEE Trans. Geoscience and Remote sensing, submitted, 2002.

[4] M. Marom, R. M. Goldstein, E. B. Thornton, and L. Shemer, "Remote sensing of ocean wave spectra by interferometric synthetic aperture radar," Nature, Vol. 345, pp. 793-795, 1990.

[5] D. Moller, S. J. Frasier, D. L. Porter, and R. E. McIntosh, "Radar-derived interferometric surface currents and their relationship to subsurface current structure," J. Geophys. Res., Vol. 103, No. C6: pp. 12839-12852, 1998.

[6] P. W. Vachon, J. W. M. Campbell, A. L. Gray, and F. W. Dobson, "Validation of along-track interferometric SAR measurements of ocean surface waves," IEEE Trans. Geoscience and Remote sensing, Vol. 37, No. 1, pp. 150-162, 1999.

[7] W. Alpers, and C. Rufenach, "The effect of orbital motions on synthetic aperture radar imagery of ocean waves," IEEE Trans. Antennas Propag., AP-27(5), pp. 685-690, 1979.